

Aeolian transport of cohesive sand

Alexandre Valance^{1,*}, Jean-Baptiste Besnard¹, Houssem Selmani², Pascal Dupont³, and Ahmed Ould El Moctar⁴

¹ Univ Rennes, CNRS UMR 6251, Institut de Physique de Rennes, Rennes 35042, France

² Université Ferhat Abbas, Institut d'Optique et de Mécanique de Précision, Sétif, Algeria

³ Univ Rennes, INSA Rennes, LGCGM, Rennes 35043, France

⁴ Univ Nantes, CNRS UMR 6607, Laboratoire Thermique et Energie de Nantes, Nantes 44306, France

Abstract. The influence of moisture on wind-driven sand transport is particularly important in coastal environments. While moisture is generally low in desert sands, it significantly affects sand transport on beaches or in coastal dune dynamics. Studies on the impact of moisture are far from yielding consistent results because it is difficult to control and measure moisture levels due to evaporation. We circumvent this difficulty by using sand-oil mixtures which offers the advantage to get rid of evaporation. With these, we conducted wind-tunnel experiments and documented with an unprecedented accuracy the effects of cohesion on wind-blown sand.

1 Introduction

Moisture has a significant influence on the initiation of motion of sand by wind and also on the resulting spatial and temporal evolution of the sand transport rate [1]. While moisture is usually very low in sandy desert areas and can be disregarded [2], aeolian sand transport on sandy beaches or in the context of coastal dune morphodynamics is expected to be crucially dependent on the moisture content within the sand. The literature regarding the impact of the moisture on wind blown sand is sparse, and available data [3–7] present considerable discrepancies regarding the magnitude of the moisture effects. These discrepancies highlight that it is experimentally difficult to control the moisture levels within the sand because of evaporation. To circumvent this difficulty, we carried wind-tunnel experiments with sand-oil mixtures instead of sand-water mixtures. Oil plays the same role as water in generating cohesion but has the significant advantage to have a very low evaporation rate in the standard conditions of temperature and pressure.

With these sand-oil mixtures, we were able to document with an unprecedented accuracy the magnitude of the cohesion effects on (i) the aerodynamic and impact thresholds [8, 9], (ii) the transient to reach an equilibrium regime and (iii) the mass transport rate at equilibrium. We found in particular that for moderate cohesion (i.e., for cohesion number less than unity), the dynamic threshold is unchanged while the static threshold increases linearly with the liquid content. Experiments also indicate that the equilibrium length necessary to reach a steady and fully developed transport regime is increased with increasing cohesion and the mass transport rate at equilibrium is the same as for cohesion-less systems.

The paper is organized as follows. In section 2, we present briefly the wind-tunnel facility and describe how we made the sand-oil mixtures. Section 3 summarizes the results concerning the effects of cohesion on erosion thresholds which have been published recently in [8, 9]. Section 4 presents partial but novel results on transient and saturated state. Finally, we conclude in Section 5.

2 Experimental setup and granular systems

2.1 Cohesive sand

This study investigates the influence of cohesion on sand transport. Specifically, in a particle-liquid mixture, cohesion arises between contacting particles through liquid bridges. The use of water in such mixtures causes problems due to evaporation during experiments. To avoid these problems [8, 9], a sand-oil mixture was used. We employed Nemours sand (Sibelco NE34) with a median diameter $d = 200\mu\text{m}$. The oil is a Sigma-Aldrich AR 20 Silicone oil characterized by a density $\rho_{oil} = 1\text{ g/ml}$, a cinematic viscosity $\nu_{oil} = 20\text{ mm}^2/\text{s}$ and a surface tension $\Gamma_{oil} = 20\text{ mN/m}$ ¹.

The preparation of the mixture is facilitated by the fact that the oil has a good affinity with silica sand. A prescribed mass of dry sand is first placed in mixer and oil is gradually introduced. Mixtures with different oil contents ω ranging from 0.05 to 3% in mass (see Table 1). were investigated.

¹The kinematic viscosity of oil is an order of magnitude higher than that of water, while its surface tension is approximately four times lower. As a result, direct comparisons between sand-water and sand-oil mixtures should be made with caution.

*e-mail: alexandre.valance@univ-rennes.fr

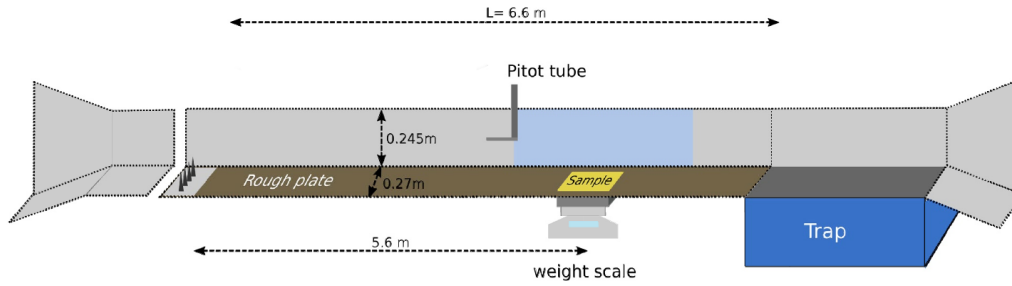


Figure 1. Wind tunnel facility used in the configuration for estimating the aerodynamic and impact erosion rate [9]: The sand bed is limited to a small square box which is weighed during the experiment.

2.2 Wind-tunnel facility

The experiments were carried out in a wind tunnel with a 6.6 m length working section and a 0.245 m × 0.27 m cross-section (see Figure 1). Two different bed configurations were used.

Box configuration: To investigate the aerodynamic and impact threshold, the sand bed was reduced to a box with a square section of dimensions 0.15 m × 0.15 m and a depth of 0.02 m. The sand sample was placed 5.6 m downstream the entrance of the wind tunnel and its surface is at the same level as the wind-tunnel floor so that there is no discontinuity (see Fig. 1). The floor of the wind tunnel (i.e., upstream and downstream of the sand bed) was made rough by gluing sand particles of the same nature as the sand bed. The sand bed was weighed continuously during the experiment by means of a scale with a milligram accuracy². This allows to record the erosion rate in the course of time either by the direct action of the turbulent flow or by the impact of particles introduced in the wind tunnel upstream with a prescribed and steady mass flow rate Q_{in} . Lastly, it is important to emphasize that the duration of the experiments is sufficiently short to ensure that the sand bed surface remains flat at the grain scale.

Sand bed configuration: To study the equilibrium state of transport, the tunnel was covered by a sand bed of finite length X from $X_{min} = 0.5$ m to $X_{max} = 6.6$ m. The granular bed had a uniform initial height of 2 cm.

Air profile: The free air flow velocity U_{∞} can be varied from 4 m/s to 38 m/s. The air flow velocity profile upstream the sand bed was characterized with Pitot tubes displayed at different heights. The profile obeys a classical logarithmic law characterized by a friction velocity u^* proportional to the free stream velocity: $u^* = 0.0388 U_{\infty}$.

3 Erosion thresholds

3.1 Aerodynamic erosion

To determine the critical friction velocity u_{sw}^* at which turbulent airflow begins to erode the sand bed, we employed a weighing-based method [8]. Specifically, we measured

²The signal of the weighing scale is biased by the pressure fluctuations of the turbulent flow. However, since the average flow pressure remains constant over time, such fluctuations can be mitigated through appropriate signal filtering.

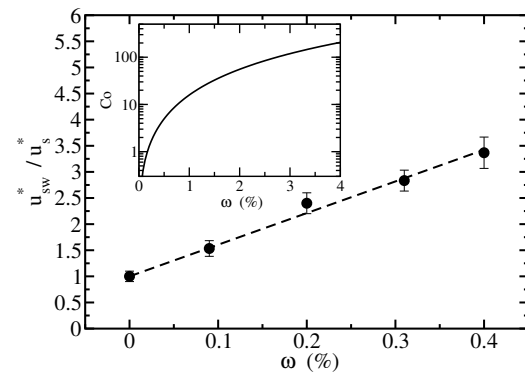


Figure 2. Aerodynamic erosion threshold u_{sw}^* (rescaled by the critical value u_s^* for a cohesionless bed) as a function of the liquid content ω . The dashed line corresponds to a linear fit to the data: $u_{sw}^* \approx u_s^*(1 + 6\omega)$. Inset: Cohesion number as a function of the liquid content (see Eq. 2). Data are taken from [9].

the aerodynamic erosion rate E_{aero} by weighing the sand-box after one minute of airflow at progressively increasing flow intensities. The threshold velocity u_{sw}^* was then identified as the point where the erosion rate exceeds a small but nonzero value: $E_{aero} \approx 5 \cdot 10^{-3} \text{ g/m}^2 \text{ s}$.

The dependence of u_{sw}^* on the liquid content ω is shown in Fig. 2. We observe a linear relationship with ω [8, 9]:

$$u_{sw}^* \approx u_s^*(1 + 6\omega), \quad (1)$$

where u_s^* denotes the critical friction velocity for a dry, cohesionless sand bed. While this linear trend is robust, its physical origin remains to be fully understood.

Using the aerodynamic threshold velocity, we can estimate the order of magnitude of the mixture's cohesive strength. To this end, we define a dimensionless cohesion number Co , which represents the ratio of the average interparticle cohesive force to the grain's weight. By balancing the forces acting on a surface grain, the cohesion number Co can be related to the aerodynamic threshold velocity [6] as follows:

$$Co \equiv \frac{F_c}{(\pi/6)\rho_p g d^3} \approx \frac{1}{3} \left(\left(\frac{u_{sw}^*}{u_s^*} \right)^2 - 1 \right) \approx \frac{1}{3} \left((1 + 6\omega)^2 - 1 \right) \quad (2)$$

In the case of a quasi-static deformation of the sand bed as expected near the aerodynamic threshold, the average

inter-particle cohesive force F_c is primarily driven by the liquid's surface tension and the liquid content. The force is expected to vary from 0 to $\Gamma_{oil}(d/2)$ with increasing liquid content. It vanishes when all contacts are dry and reaches $\Gamma_{oil}(d/2)$ when all contacts are bridged by liquid menisci. As the liquid content increases, the fraction of wet contacts and consequently the average cohesive force and the cohesion number increase accordingly.

3.2 Impact erosion

To assess the impact erosion rate E_{imp} of the sand box when it is impacted by sand particles, we impose a small but finite incoming particle flow rate Q_{in} at the entrance of the wind tunnel with the help of a hopper placed on the ceiling of the tunnel. The hopper delivers a steady mass flow rate $Q_{in} = 0.67 \text{ g/s}$. The grains released at the entrance of the wind tunnel experience a hopping motion over the upstream rigid bed, get quickly in equilibrium with the air flow and eventually impact the sand box. The erosion rate depends both on the mean velocity u_p of the impacting particles and the number n_p of particles impacting the sand box per unit time and surface. For a prescribed upstream mass flux Q_{in} , these two quantities vary with the air flow strength in opposite manner: u_p increases with increasing air flow speed while n_p decreases. The dependence of u_p and n_p with the friction velocity u^* were determined through particle tracking techniques [8, 9]. In particular, it was found that u_p is an affine function of the air flow friction velocity u^* . Experiments are run above the critical rebound shear velocity [10, 11] to prevent deposition and ensure that the mass flux Q_{in} prescribed by the hopper at the entrance of the tunnel is transported along the wind-tunnel. In practice, we use air friction speeds greater or equal than 0.15 m/s .

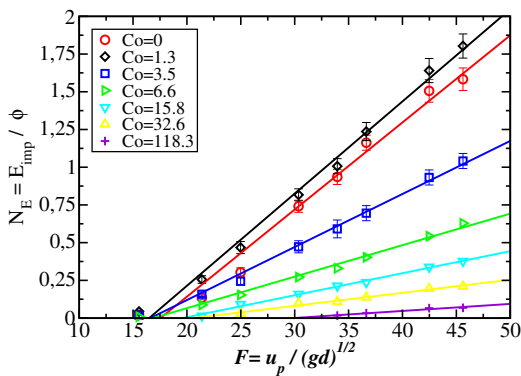


Figure 3. Rescaled impact erosion rate E_{imp}/Φ as a function of the Froude number for different cohesion numbers. To avoid cluttering the figure, error bars are displayed only for the three smallest values of the cohesion number. Data are taken from [9].

The impact erosion rate E_{imp} is determined by weighing the sand box after a finite duration of particle impingement (typically between 1 and 2 minutes) at given wind speed U_∞ with a given incoming mass flux Q_{in} . The wind speed is then increased by increment to get the impact ero-

sion rate as a function of the friction speed u^* and the experiments are repeated for different mixtures.

The quantity of interest which is measured is the impact erosion rate rescaled by the impinging mass flux $\Phi = m n_p$ (where m is the mass of a sand grain):

$$E_{imp}/\Phi = N_E . \quad (3)$$

The rescaled impact erosion rate N_E can be simply interpreted as the average number of ejected grains per impact produced by the impacting particles.

In the cohesionless case, the rescaled erosion rate can be accurately described by a linear (affine) function of the impact Froude number $\mathcal{F} = u_p / \sqrt{gd}$:

$$N_E \approx \mathcal{N}_0 (\mathcal{F} - \mathcal{F}_c) \quad (4)$$

with $\mathcal{N}_0 \approx 0.067$ and $\mathcal{F}_c \approx 18$. Here, \mathcal{N}_0 represents the impact efficiency, while \mathcal{F}_c corresponds to the critical Froude number marking the onset of particle ejection. Below this threshold, no particle ejection occurs. This linear behavior holds within a limited range of Froude numbers, specifically for $\mathcal{F}_c < \mathcal{F} < 50$.

For cohesive mixtures, the rescaled impact erosion rate as a function of the Froude number is shown in Fig. 3. The first notable observation is that the erosion rate retains an affine dependence on the Froude number and can still be described by Eq. 4, albeit with modified values of the parameters \mathcal{N}_0 and \mathcal{F}_c , which now depend on the mixture's cohesive strength. Based on this behavior, three distinct regimes of impact erosion can be identified, as detailed below.

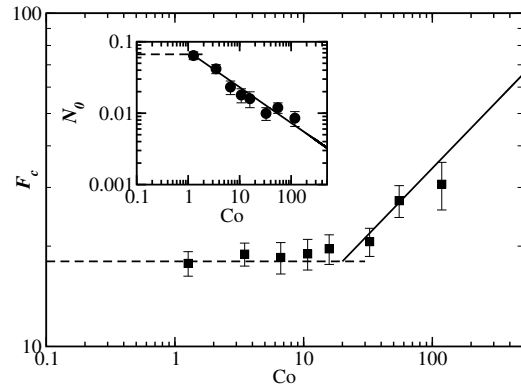


Figure 4. Variation of the critical Froude number \mathcal{F}_c and the slope \mathcal{N}_0 (see inset) as a function of the cohesion number. The horizontal dashed lines correspond to the cohesionless limit whereas the solid lines stand for the best fits using the following scaling laws: $\mathcal{N}_0 \propto Co^{-\alpha_1}$ and $\mathcal{F}_c \propto Co^{\alpha_2}$ with $\alpha_1 \approx 0.5$ and $\alpha_2 \approx 0.4$. Data are taken from [9].

For low cohesion numbers—typically when $Co \leq Co_{c_1}$ with $Co_{c_1} \approx 1$; see Fig. 4—the impact erosion rate does not show any significant deviation: both \mathcal{N}_0 and \mathcal{F}_c remain nearly unchanged.³ Interestingly, for the lowest measured cohesive case ($Co = 1.3$), the impact efficiency

³Actually, we do not have data between $Co = 0$ and $Co = 1.3$; thus, further experiments are needed to confirm this trend.

is slightly higher than in the cohesionless case (0.071 vs. 0.067). At present, this increase remains unexplained. In the intermediate cohesion regime ($Co_{c1} \leq Co \leq Co_{c2}$ with $Co_{c2} \approx 20$; see Fig. 4), the efficiency of impact erosion begins to decline. This is reflected by a reduction in the coefficient N_0 , while the critical impact Froude number \mathcal{F}_c stays approximately constant. In the regime of strong cohesion ($Co > Co_{c2}$) impact erosion is significantly reduced, as evidenced by both a decrease in N_0 and an increase in the critical Froude number \mathcal{F}_c .

A final important point should be noted: during the impact and ejection processes, viscous effects associated with the rupture of liquid bridges may play a non-negligible role. As a result, granular mixtures containing water or silicone oil could exhibit different impact erosion behaviors.

4 Transient and saturation

Using the bed configuration, we were able to characterize the transient to the saturated regime of transport for cohesive sand beds. We present here preliminary but new results. Figure 5 shows the evolution of the mass flow rate with the upstream distance X along the bed for dry sand and the two cohesive mixtures ($\omega = 0.05$ and 0.1% corresponding to $Co \approx 0.23$ and 0.52 , respectively) for a given air flow speed $U_\infty \approx 7.8 \text{ m/s}$. At this air flow speed,

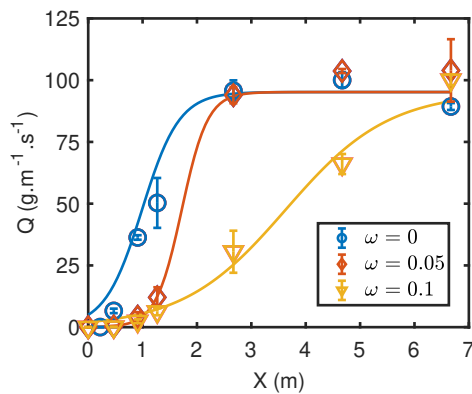


Figure 5. Evolution of the mass flow rate with upstream distance X along the bed for three different mixtures corresponding to $\omega = 0, 0.05$ and 0.1% : $U_\infty \approx 7.8 \text{ m/s}$.

the experiments indicate that the saturated mass flux is reached before the end of the wind tunnel for the cohesionless and the two cohesive sand beds and that the relaxation length (i.e., the distance required to reach a fully developed mass flow rate) increases with increasing cohesion strength. Importantly, the saturated flux seems to be independent of the cohesive strength in the range of cohesion number investigated so far. In other words, for low cohesion $Co < 1$ (where impact erosion is not affected by

cohesion), the saturated sand flux is the same for cohesionless and cohesive bed. The only change is the increase of the relaxation length required to reach the saturated state.

5 Conclusion

We characterized the effects of cohesion on the transport of sand by wind using sand-oil mixtures. The use of oil instead of water allows an accurate control of the liquid content and consequently of the cohesion level of the sand. We determined how aerodynamic and impact erosion processes are altered according to the cohesion level and subsequently showed that for low cohesion level, the mass flow rate in the steady and fully developed state of transport is identical to that obtained with a cohesionless sand bed. The only change in the low cohesion regime is the increase of the distance necessary to reach the saturated state which can be explained by the mitigation of the aerodynamic erosion process. These new experimental outcomes should provide guidance to develop theoretical model for aeolian sand transport in the context of moist sand.

References

- [1] S. Namikas, D. Sherman, A Review of the Effects of Surface Moisture Content on Aeolian Sand Transport (Springer Netherlands, Dordrecht, 1995), pp. 269–293
- [2] R. Bagnold, The physics of blown sand and desert dunes (Methuen, Londres, 1941)
- [3] W. Chepil, Soil Science Society of America Journal **20**, 288 (1956).
- [4] P. Belly, Sand movement by wind, united states army corps of engineers, vol i, Coastal Engineering Research Center, Technical Memorandum, Washington (1964).
- [5] S. Hotta, S. Kubota, S. Katori, K. Horikawa, Sand Transport by Wind on a Wet Sand Surface (1984), pp. 1265–1281
- [6] C. McKenna-Neuman, W.G. Nickling, Canadian Journal of Soil Science **69**, 79 (1989).
- [7] R. Davidson-Arnott, Y. Yang, J. Ollerhead, P.A. Hesp, I. Walker, Earth Surface Processes and Landforms: The Journal of the British Geomorphological Research Group **33**, 55 (2008).
- [8] J.B. Besnard, P. Dupont, A.O. El Moctar, A. Valance, Journal of Geophysical Research: Earth Surface **127**, e2022JF006803 (2022).
- [9] H. Selmani, J.B. Besnard, A. Ould El Moctar, P. Dupont, A. Valance, Phys. Rev. E **110**, 014901 (2024).
- [10] T. Pähtz, A.H. Clark, M. Valyrakis, O. Durán, Reviews of Geophysics **58**, e2019RG000679 (2020).
- [11] T. Pähtz, Y. Liu, Y. Xia, P. Hu, Z. He, K. Tholen, Journal of Geophysical Research: Earth Surface **126**, e2020JF005859 (2021).